

# The ROSAT Brightest Cluster Sample (BCS) — IV. The extended sample

H. Ebeling<sup>1,2,3</sup>, A.C. Edge<sup>2</sup>, S.W. Allen<sup>2</sup>, C.S. Crawford<sup>2</sup>, A.C. Fabian<sup>2</sup>, J.P. Huchra<sup>4</sup>

<sup>1</sup> *Max-Planck-Institut für extraterrestrische Physik, Giessenbachstr., D-85740 Garching, Germany*

<sup>2</sup> *Institute of Astronomy, Madingley Road, Cambridge CB3 0HA, UK*

<sup>3</sup> *Institute for Astronomy, 2680 Woodlawn Dr, Honolulu HI 96822, USA; email: ebeling@ifa.hawaii.edu*

<sup>4</sup> *Harvard-Smithsonian Center for Astrophysics, 60 Garden Street, Cambridge, MA 02138, USA*

To appear in MNRAS

## ABSTRACT

We present a low-flux extension of the X-ray selected ROSAT Brightest Cluster Sample (BCS) published in Paper I of this series. Like the original BCS and employing an identical selection procedure, the BCS extension is compiled from ROSAT All-Sky Survey (RASS) data in the northern hemisphere ( $\delta \geq 0^\circ$ ) and at high Galactic latitudes ( $|b| \geq 20^\circ$ ). It comprises 100 X-ray selected clusters of galaxies with measured redshifts  $z \leq 0.3$  (as well as seven more at  $z > 0.3$ ) and total fluxes between  $2.8 \times 10^{-12}$  erg cm<sup>-2</sup> s<sup>-1</sup> and  $4.4 \times 10^{-12}$  erg cm<sup>-2</sup> s<sup>-1</sup> in the 0.1–2.4 keV band (the latter value being the flux limit of the original BCS). The extension can be combined with the main sample published in 1998 to form the homogeneously selected extended BCS (eBCS), the largest and statistically best understood cluster sample to emerge from the ROSAT All-Sky Survey to date.

The nominal completeness of the combined sample (defined with respect to a power law fit to the bright end of the BCS  $\log N - \log S$  distribution) is relatively low at 75 per cent (compared to 90 per cent for the high-flux sample of Paper I). However, just as for the original BCS, this incompleteness can be accurately quantified, and thus statistically corrected for, as a function of X-ray luminosity and redshift.

In addition to its importance for improved statistical studies of the properties of clusters in the local Universe, the low-flux extension of the BCS is also intended to serve as a finding list for X-ray bright clusters in the northern hemisphere which we hope will prove useful in the preparation of cluster observations with the next generation of X-ray telescopes such as *Chandra* or *XMM-Newton*.

An electronic version of the eBCS can be obtained from the following URL: [www.ifa.hawaii.edu/~ebeling/clusters/BCS.html](http://www.ifa.hawaii.edu/~ebeling/clusters/BCS.html).

**Key words:** galaxies: clustering – X-rays: galaxies – surveys

## 1 INTRODUCTION

Until recently, the compilation of large statistical samples of clusters of galaxies was a task accomplishable only at optical wavelengths where photographic plates provide both all-sky coverage and sufficient depth to detect clusters at redshifts of  $z \lesssim 0.3$  (e.g., Abell 1958, Zwicky et al. 1961–1968, Abell, Corwin & Olowin 1989). Only with the completion of the ROSAT All-Sky Survey (RASS) in 1991 (Voges 1992, Trümper 1993) did unbiased large compilations of X-ray detected clusters become a feasible alternative.

To date, three X-ray flux limited cluster samples have been published from RASS data. The all-sky sample of the 242 X-ray Brightest Abell-type Clusters (XBACs) of Ebeling et al. (1996) was

the first statistical sample of X-ray bright clusters to emerge from the RASS. However, although X-ray flux limited, the XBACs sample is, by design, limited to Abell clusters and thus still affected by the biases inherent in optical cluster surveys. The other two large-scale RASS cluster samples are truly X-ray selected though: the ROSAT Brightest Cluster Sample (BCS, Ebeling et al. 1998, Paper I) comprises 203 X-ray selected clusters in the northern hemisphere, and the RASS1 Bright Sample (RASS1-BS, De Grandi et al. 1999) consists of 130 such clusters in the southern hemisphere. A fourth RASS cluster sample covering most of the southern extragalactic sky is under compilation (Böhringer et al, in preparation). In the following we briefly summarize the key features of the BCS.

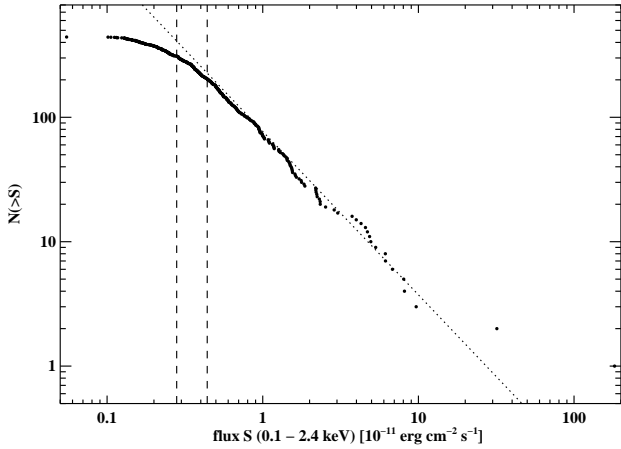


**Figure 1.** The cumulative flux distribution of all 442 clusters in our sample of VTP detections with raw count rates greater than  $0.07 \text{ count s}^{-1}$ . The dotted line represents the power law description of the BCS  $\log N - \log S$  distribution as determined in Paper I. The dashed lines mark the flux limits of the original BCS and the extended sample (eBCS) defined by the requirement of 90 and 75 per cent completeness, respectively.

## 2 THE ROSAT BRIGHTEST CLUSTER SAMPLE (BCS)

The BCS is the first truly X-ray selected, and so far largest, cluster sample to emerge from the RASS. The BCS, as listed in Paper I, comprises 203 RASS selected galaxy clusters in the northern hemisphere ( $\delta \geq 0^\circ$ ) and at high Galactic latitudes ( $|b| \geq 20^\circ$ ). All 203 BCS clusters have measured redshifts of  $z \leq 0.374$ ; the 201 BCS clusters at  $z \leq 0.3$  form the statistical subsample which is nominally 90% flux complete.

The primary selection criterion for the BCS is X-ray extent as measured in the RASS with the Standard Analysis Software System (SASS) used in the original analysis of the raw data. Since clusters of galaxies are, even at the moderate resolution of the RASS, generically extended X-ray sources at essentially all redshifts, this approach should reliably select all clusters<sup>\*</sup>. Unfortunately, the SASS source detection algorithm is known to erroneously misclassify a significant fraction of clusters as point sources. As demonstrated in the appendix of Paper I, a RASS cluster sample based exclusively on SASS source extent will miss 25% of all clusters at all redshifts, nearly independent of the imposed X-ray flux limit. ‘Pure’ X-ray selection by source extent is thus bound to result in significant incompleteness. In the compilation of the BCS we overcome this limitation of the SASS by adding to the clusters found through their SASS extent all X-ray detections (irrespective of alleged X-ray extent) of Abell and Zwicky clusters. We also perform a comprehensive reanalysis of the raw RASS photon data around all SASS detected clusters (the total sky area thus processed amounts to one sixth of the BCS survey area) with VTP (Voronoi Tessellation and Percolation, Ebeling & Wiedenmann 1993), a source detection algorithm developed and optimized specifically for the detection and characterization of irregular, extended X-ray emission from galaxy clusters. This step is crucial in two respects. Firstly, it yields accurate total cluster fluxes and, secondly, it ensures that the BCS, contrary to other RASS cluster projects, does not exclusively rely on detections made by a point source detection algorithm. It is the

<sup>\*</sup> A small number of other extended X-ray sources, such as supernova remnants, can be eliminated easily

additional clusters detected in this second processing that allow us to quantify and correct for the incompleteness and bias introduced by the imperfections of the initial point source detection algorithm.

As a result of this strategy, details of which can be found in Paper I, the BCS is currently not only the largest but, perhaps more importantly, also the statistically best understood RASS cluster sample. The BCS has been used for a wide range of astrophysical studies, including investigations of the spectral properties of central cluster galaxies (Allen et al. 1992, Crawford et al. 1995, 1999), the currently best determination of the cluster X-ray luminosity function at  $z \leq 0.3$  (Ebeling et al. 1997) and the bright end of the cluster X-ray  $\log N - \log S$  distribution (Ebeling et al. 1998). The BCS is also used routinely in studies of cluster evolution to define properties of the cluster population in the local universe (e.g., Kitayama, Sasaki & Suto 1998, Rosati et al. 1998, Jones et al. 1998, Blanchard & Bartlett 1998, Vikhlinin et al. 1999, Reichert et al. 1999, Nichol et al. 1999, Ebeling et al. 2000).

Work in progress investigates the cosmological implications of the BCS X-ray luminosity function in the framework of a Press-Schechter model (Ebeling et al., in preparation) and the three-dimensional large-scale distribution of clusters via the cluster-cluster correlation function (Edge et al., in preparation). Both of these studies use the extended BCS as defined and described below.

As in Paper I, we assume an Einstein-de Sitter Universe with  $q_0 = 0.5$  and  $H_0 = 50 \text{ km s}^{-1} \text{ Mpc}^{-1}$  throughout.

## 3 THE BCS EXTENSION

The flux limit of the BCS extension is defined crudely by the requirement that the supplementary sample comprise about 100 clusters below the flux limit of the main sample released in 1998<sup>†</sup>. Following the same procedure as for the original BCS we find this requirement to be met for a flux limit of the extended BCS (eBCS) of  $2.8 \times 10^{-12} \text{ erg cm}^{-2} \text{ s}^{-1}$  (0.1–2.4 keV), corresponding to a flux completeness of 75 per cent. The correspondence between completeness and X-ray flux limit is illustrated in Figure 1 which, similar to Fig. 20 of Paper I, shows the observed BCS  $\log N - \log S$  distribution, as well as the power law fit to the same distribution after corrections for incompleteness have been applied (see Paper I for details). The eBCS flux limit is defined by the X-ray flux (note that these are total cluster fluxes) at which the observed distribution falls below 3/4 of the value predicted by the power law description of the cumulative flux distribution for a complete sample.

The BCS extension thus defined comprises 107 clusters from the total sample of 442 clusters found in the RASS data during the compilation of the BCS. All 107 have measured redshifts of  $z \leq 0.418$ ; 100 of them fall within the redshift limit of the complete sample at  $z \leq 0.3$ . By design, the X-ray fluxes of the clusters in the extension range from  $2.8 \times 10^{-12} \text{ erg cm}^{-2} \text{ s}^{-1}$  to  $4.4 \times 10^{-12} \text{ erg cm}^{-2} \text{ s}^{-1}$  in the 0.1–2.4 keV band (the latter value being the flux limit of the original BCS).

Table 1 lists the 107 clusters in the BCS extension in analogy to Table 3 of Paper I, i.e., the contents of this table are

column 1: redshift, contamination, extent, and serendipity flag.  
Clusters at  $z > 0.3$  are marked  $\star$ ; ‘c’ means a significant fraction of the quoted flux may come from

<sup>†</sup> An agreement with MPE requires the authors to limit the total size of the BCS as published to about 300 clusters.

embedded point sources; ‘V’ (‘S’) signals significant X-ray extent according to VTP (SASS), i.e., an extent value in excess of 35 arcsec; systems flagged by a ● symbol are serendipitous VTP detections in the sense of Section 7.1 of Paper I.

- column 2: cluster name. Where clusters appear to consist of two components, two entries (‘a’ and ‘b’) are listed. We adopt cluster names in the following order of priority: Abell name, Zwicky name, other cluster name established in the literature, ROSAT RXJ name.
- column 3: right ascension (J2000) of the X-ray position as determined by VTP.
- column 4: declination (J2000) of the X-ray position as determined by VTP.
- column 5: column density of Galactic Hydrogen from Stark et al. (1992).
- column 6: total RASS exposure time.
- column 7: PSPC count rate in PHA channels 11 to 235 originally detected by VTP.
- column 8: equivalent radius  $\sqrt{A_{VTP}/\pi}$  of the source detected by VTP.
- column 9: final PSPC count rate in Pulse Height Analyzer (PHA) channels 11 to 235 based on the original VTP count rate. Statistical corrections for low-surface brightness emission that has not been detected directly and for contamination from point sources have been applied.
- column 10: error in the final PSPC count rate according to equation 4 of Paper I. The fractional uncertainty in the energy flux (column 13) and the X-ray luminosity (column 14) can be assumed to be the same as the fractional count rate error.
- column 11: ICM gas temperature used in the conversion from count rates to energy fluxes. ‘e’ indicates the temperature has been estimated from the  $L_X - kT$  relation.
- column 12: measured redshift.
- column 13: unabsorbed X-ray energy flux in the 0.1 to 2.4 keV band.
- column 14: intrinsic X-ray luminosity in the 0.1 to 2.4 keV band (cluster rest frame).
- column 15: reference for the redshift in column 12.

One of the clusters listed in Table 1, A1758a, was already listed in Table 3 of Paper I because it made the flux limit of the original sample when combined with its X-ray fainter companion A1758b. The latter falls below the flux limit of both the original and the extended BCS.

The distribution of the full eBCS sample of 310 clusters in luminosity-redshift space is shown in Fig. 2. While 211 (68%) of these are Abell clusters, the number of non-Abell clusters in the eBCS is substantial: 42 (14%) systems are Zwicky clusters without Abell identification, and another 57 (18%) are listed in neither of the two largest optical cluster catalogues. As expected, the Abell content of the eBCS is thus somewhat lower than, but still similar to, the one found for the BCS where the fractional content in Abell, Zwicky and other clusters was measured to be 70, 11, and 19 per cent.

The redshift distribution of the 310 clusters of the extended BCS shows striking signs of large-scale structure as already noted in the original BCS. Figure 3 shows the eBCS redshift histogram compared to the distribution expected for a spatially homogenous sample. The pronounced peaks at  $z \sim 0.036$  and  $z \sim 0.077$ , as

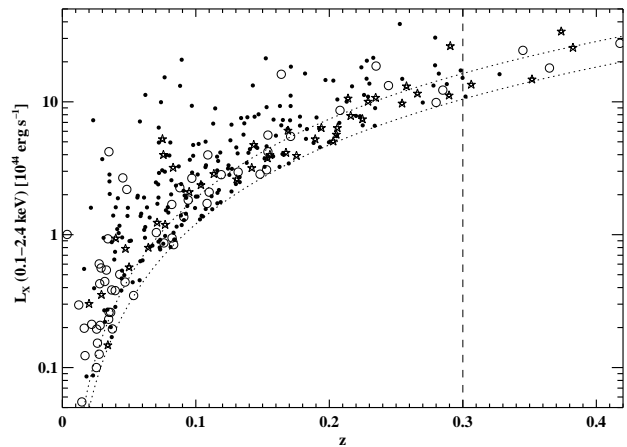


**Figure 2.** The X-ray luminosity of the 310 clusters of the 75 per cent complete flux limited eBCS as a function of redshift. The dotted lines show the cutoff introduced by the X-ray flux limits at  $2.8 \times 10^{-12} \text{ erg cm}^{-2} \text{ s}^{-1}$  (75 per cent completeness) and  $4.4 \times 10^{-12} \text{ erg cm}^{-2} \text{ s}^{-1}$  (90 per cent completeness, Paper I). Abell (Zwicky) clusters are plotted as solid dots (stars); the remaining 57 clusters not contained in these largest optical cluster catalogues are shown as open circles.

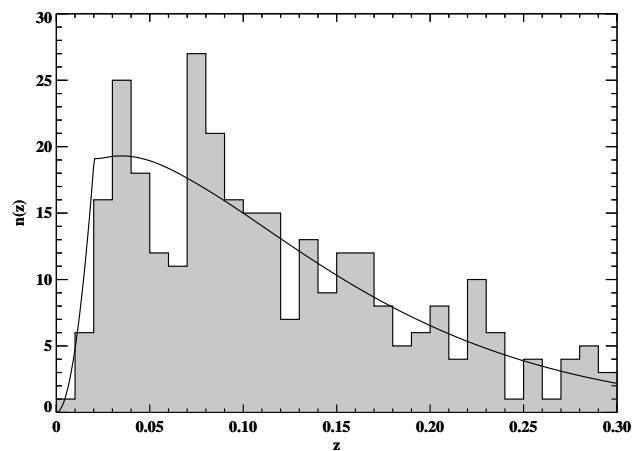


**Figure 3.** The differential redshift distribution of the clusters in the extended BCS. The solid curve shows the redshift distribution expected for a spatially homogeneous cluster distribution.

well as the depletion between them, are prominent also in the redshift distribution of the original BCS (see Section 8.1 of Paper I). As shown in Paper I, the excess of clusters at these redshifts can not be attributed to any single supercluster but is generated by clusters and superclusters distributed widely over the solid angle covered by the BCS.

An overview of the distribution of the eBCS on the sky is shown in Fig. 4.

#### ACKNOWLEDGEMENTS

The authors are indebted to the ROSAT team at MPE for providing the RASS photon data this analysis is based upon. The identification of non-cluster sources that contaminated the sample we originally started from was greatly facilitated by the availability

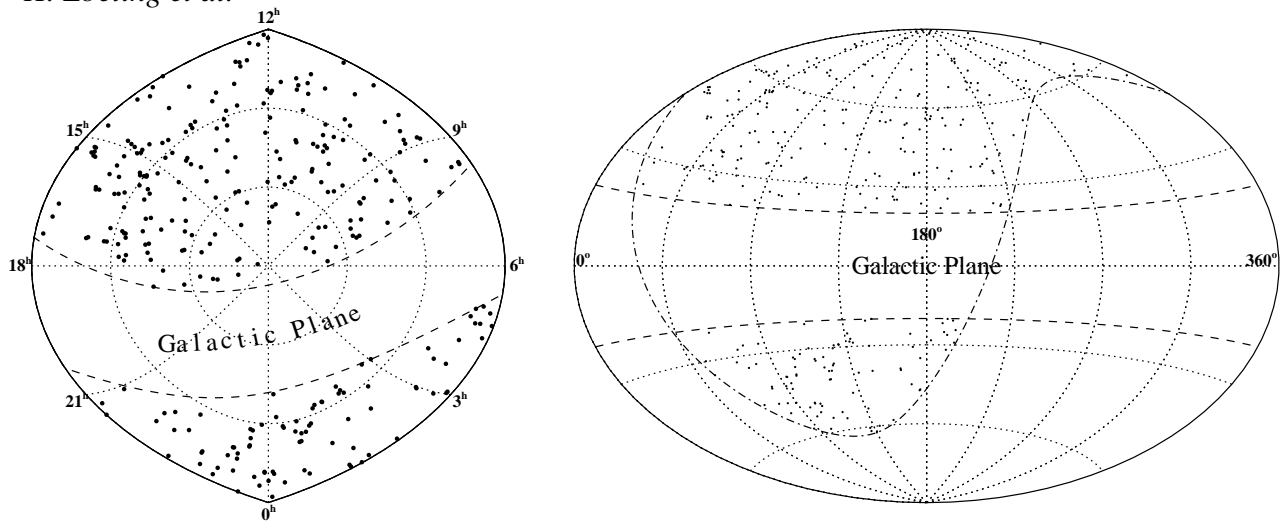


**Figure 4.** The distribution of the 301 eBCS clusters ( $z \leq 0.3$  only) on the sky in a view of the northern equatorial hemisphere (left) and in Galactic coordinates (right). Equal-area Aitoff projections are used in both plots. The 40 deg wide exclusion zone around the Galactic equator is marked by the dashed lines. Also marked as a dot-dashed line in the right panel is the line of  $\delta = 0^\circ$ .

of digitized optical images from the POSS and UK Schmidt sky surveys obtained through STScI's DSS Web interface. All of the data analysis presented in this paper was carried out using the Interactive Data Language (IDL). We are greatly indebted to all who contributed to the various IDL User's Libraries; the routines of the IDL Astronomy User's Library (maintained by Wayne Landsman) have been used particularly extensively.

HE thanks the Time Allocation Committee of the Institute for Astronomy for their support of the spectroscopic follow-up observations of eBCS clusters. HE also gratefully acknowledges partial financial support from a European Union EARA Fellowship, SAO contract SV4-64008, and NASA LTSA grant NAG 5-8253. ACE, ACF and CSC thank the Royal Society for support.

This research has made use of data obtained through the High Energy Astrophysics Science Archive Research Center Online Service, provided by the NASA-Goddard Space Flight Center, and the NASA/IPAC Extragalactic Database (NED).

## REFERENCES

- Abell G.O., 1958, *ApJS*, 3, 211  
 Abell G.O., Corwin H.G., Olowin R.P., 1989, *ApJS*, 70, 1  
 Allen S.W. et al., 1992, *MNRAS*, 259, 67  
 Batuski D.J., Burns J.O., Newberry M.V., Hill J.M., Deeg H.-J., Laubscher Bryan.E., Elston R.J., 1991, *AJ*, 101, 1983  
 Beers T.C., Kriessler J.R., Bird C.M., Huchra J.P. 1995, *AJ*, 109, 874  
 Blanchard A. & Bartlett J.G., 1998, *A&A*, 332, L49  
 Ciardullo R., Ford H., Bartko F., Harms R. 1983, *ApJ*, 273, 24  
 Crawford C.S., Edge A.C., Fabian A.C., Allen S.W., Böhringer H., Ebeling H., McMahon R.G., Voges W., 1995, *MNRAS*, 274, 75  
 Crawford C.S., Allen S.W., Ebeling H., Edge A.C., Fabian A.C., 1999, *MNRAS*, 306, 857  
 De Grandi S. et al., 1999, *ApJ*, 514, 148  
 Ebeling H. & Wiedenmann G., 1993, *Phys. Rev. E*, 47, 704  
 Ebeling H., Voges W., Böhringer H., Edge A.C., Huchra J.P., Briel U.G., 1996, *MNRAS*, 281, 799  
 Ebeling H., Edge A.C., Böhringer H., Allen S.W., Crawford C.S., Fabian A.C., Voges W., Huchra J.P., 1998, *MNRAS*, 301, 881 (Paper I)  
 Ebeling H., Jones L.R., Fairley B., Scharf C., Perlman E., Horner D., 2000, *ApJ*, submitted  
 Fetisova T. 1982, *Sov. Astron.*, 25, 647  
 Henry J.P. & Lavery R.J., 1984, *ApJ*, 280, 1  
 Hoessel J.G., Gunn J.E., Thuan T.X. 1980, *ApJ*, 241, 466  
 Hopp U., Kuhn, B., Thiele U., Birkle K, Elsässer H., Kovachev B., 1995, *A&AS*, 109, 537  
 Huchra J.P., Henry J.P., Postman M., Geller M.J., 1990, *ApJ*, 365, 66  
 Huchra J.P., Geller M.J., Clemens C.M., Tokarz S.P., Michel A. 1992, *Bull. C.D.S.*, 41, 31  
 Jones L.R., Scharf C., Ebeling H., Perlman E., Wegner G., Malkan M., Horner D., 1998, *ApJ*, 495, 100  
 Kitayama T., Sasaki S., Suto Y., 1998, *PASJ*, 50, 1  
 Ledlow M.J. & Owen F.N., 1995, *AJ*, 110, 1959  
 Marzke R.O., Huchra J.P., Geller M.J., 1996, *AJ*, 112, 1803  
 Nichol R.C. et al., 1999, *ApJ*, 521, L21  
 Owen F.N., Ledlow M.J., Keel W.C., 1995, *AJ*, 109, 14  
 Postman M., Huchra J.P., Geller M.J. 1992, *ApJ*, 384, 404  
 Postman M. & Lauer T.R. 1995, *ApJ*, 440, 28  
 Reichart D.E., Nichol R.C., Castander F.J., Burke D.J., Romer A.K., Holden B.P., Collins C.A., Ulmer M.P., 1999, *ApJ*, 518, 521  
 Rhee G. & Katgert P. 1988, *A&AS*, 72, 243  
 Romer A.K., 1994, PhD thesis, University of Edinburgh  
 Rosati P., Della Ceca R., Norman C., Giacconi R., 1998, *ApJ*, 492, L21  
 Sarazin C.L., Rood H.J., Struble M.F. 1982, *A&A*, 108, L7  
 Schneider D.P., Gunn J.E., Hoessel J.G. 1983, *ApJ*, 264, 337  
 Shectman S.A. 1985, *ApJS*, 57, 77  
 Small T.A., Sargent W.L.W., Hamilton D., 1997, *ApJ*, 487, 512  
 Stark A.A., Gammie C.F., Wilson R.W., Bally J., Linke R.A., Heiles C., Hurwitz M., 1992 *ApJS*, 79, 77  
 Stocke J.T., Morris S.L., Gioia I.M., Maccacaro T., Schild R., Wolter A., Fleming T.A., Henry J.P. 1991, *ApJS*, 76, 813  
 Struble M.F. & Rood H.J. 1987, *ApJS*, 63, 543  
 Trümper J., 1993, *Science*, 260, 1769  
 de Vaucouleurs G., de Vaucouleurs A., Corwin H.G., Buta R.J., Paturel G., Fouqué P. 1991, *Third Reference Catalogue of Bright Galaxies*, Springer, New York  
 Vikhlinin A., McNamara B.R., Forman W., Jones C., Quintana H., Hornstrup A., 1999, *ApJ*, 491, L21  
 Voges W. 1992, *Proceedings of Satellite Symposium 3, ESA ISY-3*, p9  
 Zabludoff A.I., Huchra J.P., Geller M.J. 1990, *ApJS*, 74, 1  
 Zwicky F., Herzog E., Wild P., Karpowicz M., Kowal, C.T., 1961–1968, *Catalogue of galaxies and cluster galaxies*, Vols. 1–6

$z$ , contam. extent, serend. flag	cluster name	$\alpha$ (J2000) [deg]	$\delta$ (J2000) [deg]	$n_H$ [ $10^{20} \text{ cm}^{-2}$ ]	RASS exp. time [s]	VTP count rate [ $\text{s}^{-1}$ ]	$r_{\text{VTP}}$ [arcmin]	final count rate [ $\text{s}^{-1}$ ]	count rate error [ $\text{s}^{-1}$ ]	$kT$ [keV]	$z$	$f_X$ (0.1–2.4 keV) [ $10^{-12} \text{ erg cm}^{-2} \text{ s}^{-1}$ ]	$L_X$ (0.1–2.4 keV) [ $10^{44} \text{ erg s}^{-1}$ ]	$z$ reference
V	A2700	0.954	2.068	3.0	412	0.20	4.1	0.23	0.06	3.9 <sup>e</sup>	0.0994	3.7	1.59	(27)
VS	RXJ0004.9+1142	1.233	11.701	5.3	441	0.16	4.6	0.18	0.05	3.1 <sup>e</sup>	0.0761	3.5	0.87	(28)
VS	Z15	1.572	10.868	5.3	440	0.15	5.7	0.18	0.06	5.9 <sup>e</sup>	0.1675	3.5	4.17	(7)
V	Z28	2.237	41.177	7.3	401	0.16	4.4	0.18	0.06	5.6 <sup>e</sup>	0.1537	3.8	3.79	(7)
VS	A16	4.199	6.749	4.5	512	0.14	5.6	0.17	0.05	3.2 <sup>e</sup>	0.0838	3.0	0.92	(21)
★ VS	RXJ0027.6+2616	6.924	26.272	3.8	388	0.14	4.5	0.19	0.06	11.1 <sup>e</sup>	0.3649	3.3	17.97	(7)
V	Z193	9.149	25.744	4.0	404	0.15	5.0	0.17	0.06	1.6 <sup>e</sup>	0.0341	3.0	0.15	(7)
	Z348	16.702	1.045	3.0	434	0.21	4.1	0.22	0.06	8.4 <sup>e</sup>	0.2545	3.6	9.80	(7)
V ●	A156	17.925	33.453	5.1	472	0.16	5.7	0.19	0.06	4.5 <sup>e</sup>	0.1173	3.7	2.17	(7)
VS	RXJ0142.0+2131	25.511	21.522	6.4	406	0.13	4.1	0.15	0.05	8.5 <sup>e</sup>	0.2800	3.0	9.88	(7)
V ●	A260	27.687	33.090	4.7	344	0.15	3.7	0.19	0.07	1.8 <sup>e</sup>	0.0363	3.5	0.20	(26)
V ●	A278	29.357	32.224	5.1	321	0.14	3.5	0.18	0.07	3.5 <sup>e</sup>	0.0894	3.4	1.18	(18)
VS	A311	32.385	19.764	8.1	280	0.15	4.3	0.20	0.08	3.0 <sup>e</sup>	0.0657	4.4	0.81	(29)
S	RXJ0437.1+0043	69.285	0.728	7.7	564	0.15	3.4	0.17	0.05	9.3 <sup>e</sup>	0.2850	3.6	12.25	(7)
VS	RXJ0448.2+0953	72.054	9.890	12.2	408	0.14	4.6	0.17	0.06	5.9 <sup>e</sup>	0.1540	4.2	4.21	(7)
VS	A554	94.657	67.410	7.1	379	0.11	4.0	0.14	0.05	3.9 <sup>e</sup>	0.1123	2.9	1.55	(7)
VS	A565	107.021	71.864	4.5	453	0.12	4.4	0.16	0.05	3.7 <sup>e</sup>	0.1053	2.9	1.37	(29)
V ●	A572	108.580	54.685	5.9	393	0.11	4.1	0.15	0.06	3.7 <sup>e</sup>	0.1043	3.0	1.39	(7)
VS	A580	111.518	41.389	6.6	462	0.14	5.1	0.18	0.06	4.3 <sup>e</sup>	0.1118	3.6	1.95	(7)
S	Z1370	115.438	74.243	3.5	456	0.22	3.7	0.23	0.06	7.7 <sup>e</sup>	0.2160	4.0	7.90	(22)
	Z1432	117.850	17.513	4.4	338	0.17	2.7	0.19	0.06	6.5 <sup>e</sup>	0.1894	3.5	5.27	(7)
VS	A611	120.233	36.061	4.8	445	0.18	5.1	0.21	0.06	9.7 <sup>e</sup>	0.2880	4.0	13.60	(5)
VS	A621	122.809	70.031	3.4	474	0.19	4.4	0.22	0.06	7.6 <sup>e</sup>	0.2230	3.7	7.79	(5)
VS	RXJ0820.9+0751	125.248	7.854	2.5	332	0.23	4.3	0.26	0.08	4.4 <sup>e</sup>	0.1100	4.0	2.09	(5)
V	Z1693	126.497	4.263	2.9	314	0.18	4.1	0.21	0.07	7.5 <sup>e</sup>	0.2248	3.5	7.46	(7)
	Z1883	130.747	29.476	3.9	309	0.21	5.2	0.22	0.07	7.0 <sup>e</sup>	0.1940	4.0	6.41	(22)
V ●	A743	136.614	10.345	3.7	360	0.17	4.9	0.20	0.07	4.9 <sup>e</sup>	0.1328	3.6	2.71	(7)
VS	A744	136.857	16.654	3.5	372	0.16	4.9	0.20	0.06	3.0 <sup>e</sup>	0.0733	3.3	0.77	(22)
cVS	A779	139.922	33.763	1.7	449	0.22	5.0	0.29	0.07	1.4 <sup>e</sup>	0.0230	3.8	0.09	(12)
	Z2379	141.795	53.450	1.7	518	0.20	3.9	0.22	0.06	6.7 <sup>e</sup>	0.2052	3.2	5.71	(7)
VS	A854	145.517	8.973	3.0	290	0.20	4.4	0.23	0.08	7.3 <sup>e</sup>	0.2075	3.8	6.94	(6)
VS	A853	145.565	15.382	3.4	439	0.18	4.9	0.20	0.06	5.8 <sup>e</sup>	0.1649	3.5	4.05	(7)
★ S	Z2661	147.498	17.141	3.1	427	0.23	5.0	0.26	0.07	12.9 <sup>e</sup>	0.3825	4.3	25.75	(12)
S	RXJ1000.5+4409	150.130	44.154	1.0	510	0.24	3.6	0.25	0.06	5.2 <sup>e</sup>	0.1530	3.1	3.08	(5)
V	A910	150.773	67.156	3.5	499	0.14	4.3	0.18	0.05	6.6 <sup>e</sup>	0.2055	3.1	5.52	(23)
S	A923	151.666	25.924	2.7	348	0.20	3.9	0.22	0.07	4.4 <sup>e</sup>	0.1162	3.6	2.07	(18)
VS	A964	154.151	24.806	2.3	453	0.16	4.0	0.19	0.06	3.0 <sup>e</sup>	0.0811	2.8	0.81	(10)
VS	A971	154.980	40.996	1.3	500	0.25	5.3	0.31	0.07	3.8 <sup>e</sup>	0.0926	3.9	1.44	(5)
VS	RXJ1022.1+3830	155.539	38.502	1.4	491	0.17	4.4	0.22	0.06	2.2 <sup>e</sup>	0.0534	2.8	0.35	(12)
VS	A1035	158.059	40.247	1.3	483	0.25	5.2	0.31	0.07	3.2 <sup>e</sup>	0.0733	4.0	0.92	(23)

$z$ , contam. extent, serend. flag	cluster name	$\alpha$ (J2000) [deg]	$\delta$ (J2000) [deg]	$n_{\text{H}}$ [ $10^{20} \text{ cm}^{-2}$ ]	RASS exp. time [s]	VTP count rate [ $\text{s}^{-1}$ ]	$r_{\text{VTP}}$ [arcmin]	final count rate [ $\text{s}^{-1}$ ]	count rate error [ $\text{s}^{-1}$ ]	$kT$ [keV]	$z$	$f_{\text{X}}$ (0.1–2.4 keV) [ $10^{-12} \text{ erg cm}^{-2} \text{ s}^{-1}$ ]	$L_{\text{X}}$ (0.1–2.4 keV) [ $10^{44} \text{ erg s}^{-1}$ ]	$z$ reference
VS	A1045	158.743	30.695	1.9	468	0.25	3.4	0.29	0.07	5.4 <sup>e</sup>	0.1381	4.3	3.47	(1)
	A1126	163.453	16.842	2.2	305	0.23	3.2	0.24	0.07	3.5 <sup>e</sup>	0.0856	3.7	1.15	(23)
cV	A1139	164.612	1.594	3.9	435	0.20	5.6	0.24	0.07	2.1 <sup>e</sup>	0.0397	4.2	0.29	(10)
VS	A1173	167.325	41.569	1.6	429	0.25	4.6	0.28	0.07	3.3 <sup>e</sup>	0.0770	3.8	0.98	(12)
S	Z3916	168.596	58.387	0.7	586	0.29	4.5	0.31	0.06	7.0 <sup>e</sup>	0.2060	3.6	6.41	(5)
★	Z3959	168.972	1.510	4.2	442	0.13	3.1	0.16	0.05	10.2 <sup>e</sup>	0.3518	2.9	14.87	(7)
	A1264	171.753	17.126	2.0	443	0.19	3.8	0.21	0.06	4.4 <sup>e</sup>	0.1267	3.1	2.11	(20)
VS	A1291	173.088	55.979	0.9	403	0.28	5.0	0.32	0.08	2.4 <sup>e</sup>	0.0527	3.7	0.44	(23)
VS	A1412	178.995	73.410	2.3	760	0.19	4.4	0.23	0.05	3.3 <sup>e</sup>	0.0833	3.5	1.03	(9)
VS	Z4673	179.218	24.248	1.8	471	0.23	4.9	0.26	0.06	5.2 <sup>e</sup>	0.1419	3.7	3.20	(1)
S	A1443	180.321	23.105	2.1	463	0.19	3.7	0.21	0.06	8.5 <sup>e</sup>	0.2700	3.3	9.87	(7)
VS	A1446	180.516	58.041	1.4	488	0.18	4.3	0.22	0.06	3.7 <sup>e</sup>	0.1031	2.9	1.30	(11)
★ V ●	A1576	189.237	63.188	1.7	540	0.18	4.2	0.20	0.05	8.9 <sup>e</sup>	0.3020	2.9	10.96	(8)
S	A1602	190.868	27.286	1.2	482	0.20	4.1	0.23	0.06	6.3 <sup>e</sup>	0.1997	2.9	4.96	(7)
S	A1672	196.085	33.601	1.0	523	0.23	4.1	0.26	0.06	6.3 <sup>e</sup>	0.1882	3.3	4.90	(1)
★ cV	Z5699	196.507	26.505	0.9	502	0.24	4.5	0.28	0.07	9.8 <sup>e</sup>	0.3063	3.5	13.59	(7)
V ●	A1691	197.771	39.222	1.2	585	0.27	4.8	0.32	0.06	3.1 <sup>e</sup>	0.0720	4.0	0.89	(9)
VS	Z5768	197.884	22.009	1.8	723	0.22	5.4	0.27	0.06	9.1 <sup>e</sup>	0.2660	4.0	11.64	(7)
	A1704	198.591	64.575	1.8	607	0.24	4.0	0.26	0.06	7.7 <sup>e</sup>	0.2200	3.9	7.83	(8)
★ cVS	A1722	199.997	70.073	1.5	736	0.23	4.7	0.26	0.05	10.5 <sup>e</sup>	0.3275	3.7	16.14	(8)
V	A1728	200.876	11.296	1.8	311	0.22	3.7	0.25	0.08	3.6 <sup>e</sup>	0.0911	3.6	1.29	(7)
V	A1744	201.453	59.330	1.6	741	0.21	4.4	0.24	0.05	5.3 <sup>e</sup>	0.1515	3.3	3.24	(11)
VS	A1758a	203.189	50.548	1.1	591	0.25	4.5	0.28	0.06	9.1 <sup>e</sup>	0.2792	3.6	11.61	(1)
VS	A1814	208.499	14.924	1.7	398	0.23	4.8	0.30	0.08	5.0 <sup>e</sup>	0.1251	4.2	2.82	(24)
VS	A1895	213.551	71.260	2.0	857	0.17	4.2	0.21	0.04	7.2 <sup>e</sup>	0.2250	3.1	6.65	(8)
VS	RXJ1423.1+2616	215.799	26.276	1.6	392	0.21	4.8	0.25	0.07	1.8 <sup>e</sup>	0.0375	3.2	0.19	(3)
S	RXJ1423.9+4015	215.976	40.261	0.9	604	0.24	3.8	0.28	0.06	3.2 <sup>e</sup>	0.0822	3.2	0.94	(12)
VS	A1925	217.135	56.879	1.4	725	0.19	4.4	0.24	0.05	3.9 <sup>e</sup>	0.1074	3.2	1.56	(7)
V ●	A1961	221.094	31.235	1.3	614	0.17	4.2	0.22	0.05	7.1 <sup>e</sup>	0.2340	2.9	6.60	(6)
VS	A1986	223.292	21.897	2.8	415	0.15	4.1	0.18	0.06	4.1 <sup>e</sup>	0.1186	2.9	1.76	(4)
VS	Z7215	225.334	42.344	1.5	575	0.20	4.3	0.23	0.06	9.0 <sup>e</sup>	0.2897	3.2	11.26	(7)
VS	A2036	227.778	18.049	2.8	379	0.15	3.7	0.19	0.06	4.1 <sup>e</sup>	0.1161	3.0	1.72	(20)
cV ●	A2067	230.783	30.845	1.9	399	0.20	5.2	0.24	0.07	3.1 <sup>e</sup>	0.0756	3.5	0.86	(29)
cV ●	A2073	231.436	28.428	2.6	381	0.19	4.7	0.24	0.07	5.6 <sup>e</sup>	0.1515	3.8	3.74	(19)
S	A2146	239.040	66.355	2.8	1318	0.23	3.8	0.24	0.04	8.1 <sup>e</sup>	0.2343	3.9	8.97	(1)
VS	A2141	239.436	35.497	1.9	349	0.21	4.4	0.25	0.07	5.7 <sup>e</sup>	0.1579	3.7	3.89	(15)
VS	A2149	240.399	53.918	1.2	1122	0.28	5.1	0.34	0.05	3.0 <sup>e</sup>	0.0675	4.2	0.83	(2)
V	A2148	240.759	25.404	4.5	654	0.19	5.1	0.22	0.05	3.7 <sup>e</sup>	0.0888	4.1	1.39	(16)
V	A2152	241.384	16.442	3.4	569	0.15	4.0	0.17	0.05	1.7 <sup>e</sup>	0.0370	2.9	0.17	(23)
V ●	A2169	243.540	49.153	1.5	542	0.19	5.3	0.24	0.06	2.4 <sup>e</sup>	0.0579	3.1	0.45	(29)

$z$ , contam. extent, serend. flag	cluster name	$\alpha$ (J2000) [deg]	$\delta$ (J2000) [deg]	$n_H$ [ $10^{20}$ cm $^{-2}$ ]	RASS exp. time [s]	VTP count rate [s $^{-1}$ ]	$r_{VTP}$ [arcmin]	final count rate [s $^{-1}$ ]	count rate error [s $^{-1}$ ]	$kT$ [keV]	$z$	$f_X$ (0.1–2.4 keV) [ $10^{-12}$ erg cm $^{-2}$ s $^{-1}$ ]	$L_X$ (0.1–2.4 keV) [ $10^{44}$ erg s $^{-1}$ ]	$z$ reference
VS	A2187	246.053	41.242	0.9	906	0.26	4.4	0.30	0.05	6.5 <sup>e</sup>	0.1825	3.7	5.26	(23)
VS	A2201	246.748	55.477	1.8	874	0.20	4.1	0.23	0.04	4.7 <sup>e</sup>	0.1300	3.3	2.40	(5)
S	A2208	247.424	58.531	1.8	1386	0.20	3.7	0.23	0.04	4.7 <sup>e</sup>	0.1329	3.3	2.49	(5)
cVS	RXJ1652.6+4011	253.166	40.193	1.7	596	0.18	3.8	0.22	0.05	5.0 <sup>e</sup>	0.1481	3.1	2.85	(7)
VS	A2245	255.633	33.513	2.2	767	0.17	4.8	0.20	0.04	3.2 <sup>e</sup>	0.0843	3.0	0.92	(17)
V •	RXJ1714.3+4340	258.590	43.677	2.1	1067	0.22	5.1	0.27	0.05	1.5 <sup>e</sup>	0.0276	3.8	0.13	(14)
S	RXJ1715.2+0309	258.801	3.161	6.3	508	0.18	2.6	0.20	0.05	5.1 <sup>e</sup>	0.1317	4.0	2.96	(12)
V •	Z8182	259.043	20.357	5.2	630	0.16	4.6	0.19	0.05	4.8 <sup>e</sup>	0.1306	3.6	2.63	(7)
S	Z8193	259.329	42.444	2.2	939	0.19	3.2	0.20	0.04	5.7 <sup>e</sup>	0.1754	3.0	3.96	(1)
VS	A2271	259.621	78.029	4.0	1826	0.20	5.8	0.24	0.03	2.7 <sup>e</sup>	0.0584	4.3	0.63	(10)
VS	Z8284	266.796	45.216	2.9	1249	0.20	5.2	0.24	0.04	5.8 <sup>e</sup>	0.1555	3.9	4.01	(7)
VS	RXJ1836.5+6344	279.127	63.748	4.9	4341	0.13	4.1	0.14	0.02	3.1 <sup>e</sup>	0.0834	2.8	0.84	(7)
VS	RXJ1844.1+4533	281.033	45.554	5.6	1137	0.16	4.5	0.19	0.04	3.7 <sup>e</sup>	0.0910	3.8	1.36	(12)
VS	RXJ1852.1+5711	283.034	57.186	5.3	1417	0.15	4.2	0.18	0.03	4.1 <sup>e</sup>	0.1084	3.4	1.72	(7)
VS	A2315	285.194	69.975	6.5	2398	0.17	5.0	0.22	0.03	4.0 <sup>e</sup>	0.0936	4.4	1.64	(29)
S	Z8484	316.221	14.030	7.1	504	0.12	3.8	0.14	0.05	6.4 <sup>e</sup>	0.2029	2.9	5.08	(12)
VS	A2396	328.924	12.529	6.0	313	0.17	4.6	0.20	0.07	6.9 <sup>e</sup>	0.1924	4.0	6.28	(15)
S	A2445	336.728	25.849	5.0	519	0.16	4.6	0.18	0.05	5.8 <sup>e</sup>	0.1660	3.4	4.00	(7)
★ VS	RXJ2228.6+2037	337.154	20.623	4.4	479	0.18	6.0	0.21	0.06	13.4 <sup>e</sup>	0.4177	3.9	27.56	(7)
V •	RXJ2250.0+1137	342.523	11.617	4.8	419	0.15	7.2	0.20	0.06	1.4 <sup>e</sup>	0.0255	3.5	0.10	(25)
V	A2507	344.238	5.547	5.4	382	0.12	5.0	0.14	0.05	5.4 <sup>e</sup>	0.1696	2.8	3.44	(7)
VS	A2552	347.898	3.646	4.9	383	0.18	4.3	0.21	0.06	10.2 <sup>e</sup>	0.2998	4.1	15.15	(7)
	A2561	348.499	14.744	4.9	457	0.14	4.3	0.15	0.05	5.3 <sup>e</sup>	0.1627	2.9	3.24	(7)
S	A2588	350.907	9.154	4.6	446	0.14	4.2	0.15	0.05	6.1 <sup>e</sup>	0.1930	2.9	4.55	(7)
cV •	A2625	354.034	20.623	4.1	491	0.18	6.7	0.23	0.06	2.8 <sup>e</sup>	0.0601	4.1	0.64	(6)
S	A2631	354.417	0.276	4.1	383	0.21	4.7	0.23	0.06	9.6 <sup>e</sup>	0.2780	4.1	13.26	(5)
V	A2678	358.925	11.647	4.8	438	0.15	6.0	0.19	0.06	3.0 <sup>e</sup>	0.0729	3.5	0.80	(13)

(1) Allen et al. 1992, (2) Batuski et al. 1991, (3) Beers et al. 1995, (4) Ciardullo et al. 1983, (5) Crawford et al. 1995, (6) Fetisova 1982, (7) Ebeling & Mullis, in preparation, (8) Henry & Lavery 1984, (9) Hoessel et al. 1980, (10) J.P. Huchra, private communication, (11) J.P. Huchra et al. 1990, (12) Huchra et al. 1992, (13) Ledlow & Owen 1995, (14) Marzke, Huchra & Geller 1996, (15) Owen et al. 1995, (16) Postman & Lauer 1995, (17) Rhee & Katgert 1988, (18) Sarazin et al. 1982, (19) Small et al. 1997, (20) Schneider et al. 1983, (21) Shectman 1985, (22) Stocke et al. 1991, (23) Struble & Rood 1987, (24) E. Tago, private communication, (25) de Vaucouleurs et al. 1991, (26) Zabludoff et al. 1990, (27) Romer 1994, (28) Hopp et al. 1995, (29) Postman, Huchra & Geller 1992